

# A new velocity model for clay–sand mixtures<sup>1</sup>

Shiyu Xu<sup>2</sup> and Roy E. White<sup>2</sup>

## Abstract

None of the standard porosity–velocity models (e.g. the time-average equation, Raymer's equations) is satisfactory for interpreting well-logging data over a broad depth range. Clays in the section are the usual source of the difficulty through the bias and scatter that they introduce into the relationship between porosity and P-wave transit time. Because clays are composed of fine sheet-like particles, they normally form pores with much smaller aspect ratios than those associated with sand grains. This difference in pore geometry provides the key to obtaining more consistent resistivity and sonic log interpretations.

A velocity model for clay–sand mixtures has been developed in terms of the Kuster and Toksöz, effective medium and Gassmann theories. In this model, the total pore space is assumed to consist of two parts: (1) pores associated with sand grains and (2) pores associated with clays (including bound water). The essential feature of the model is the assumption that the geometry of pores associated with sand grains is significantly different from that associated with clays. Because of this, porosity in shales affects elastic compliance differently from porosity in sandstones. The predictive power of the model is demonstrated by the agreement between its predictions and laboratory measurements and by its ability to predict sonic logs from other logs over large depth intervals where formations vary from unconsolidated to consolidated sandstones and shales.

## Introduction

The sonic log is one of the three porosity indicators in formation evaluation. In the past, various models have been proposed in order to derive porosity directly from sonic logs (Wood 1941; Wyllie, Gregory and Gardner 1956; Raymer, Hunt and Gardner 1980; Krief *et al.* 1990). However the porosity–velocity relationship is usually scattered. Han, Nur and Morgan (1986) have shown that much of the scatter can be attributed to lithology and, more specifically, to clay content. In an

---

<sup>1</sup> Paper presented at the 54th EAGE meeting, Paris, June 1992. Received June 1993, revision accepted July 1994.

<sup>2</sup> Exploration Geophysics Group, Research School of Geological Sciences, Birkbeck College & University College London, Gower Street, London WC1E 6BT.

experimental study, Marion *et al.* (1992) observed two distinct trends in the porosity–velocity relationship: one for shaly sands and the other for sandy shales. The authors conclude that the scatter is due primarily to clay content and secondarily to compaction.

The effect of clays on elastic wave velocities was qualitatively but comprehensively discussed by Anstey (1991): “Loose clay fines in pores reduce velocity slightly, just by the density effect. If the fines are tightly packed in the pores, then it is a matter of the balance between rigidity and density of the clay material itself”. Laboratory measurements (Han *et al.* 1986; Klimentos and McCann 1990; Klimentos 1991; Marion *et al.* 1992) demonstrate that **clay has a strong effect on elastic wave velocities and wave attenuation**. However the results and their interpretations are slightly different. On the one hand, Han *et al.* (1986) and Klimentos (1991) found empirically that the P-wave velocity was a linear function of both porosity and clay content, decreasing with increasing porosity or clay content. On the other hand, Marion *et al.* (1992) observed an initial increase in P-wave velocity with clay content; this was attributed to a reduction in porosity as pore space between sand grains was replaced by clay particles. Then, after the clay content exceeded a critical value (normally between 20% and 40%), the P-wave velocity decreased with clay content; this was explained by an increase in porosity with clay content once the grain-related porosity had been lost.

Although laboratory observations have shown that clays affect elastic wave velocities significantly, very few attempts have been made to interpret mechanisms for the effect. Eastwood and Castagna (1983) attempted to relate clay effects to pore aspect ratios on the basis of the Kuster and Toksöz (1974) model and identified two cases where the interpretation of velocities in reservoir rocks may be affected by pores of low aspect ratios. One occurred in overpressured shaly formations, which were potentially influenced by cracks because of the control of effective pressure on crack closure. The other was in shaly sands, where there was uncertainty concerning the relative dominance of rounded pores and cracks.

The effect of clays on the electrical properties of porous rocks has been studied extensively. Their effect on elastic wave velocities, however, has been modelled quantitatively only recently. A number of authors (e.g. Han *et al.* 1986; Klimentos 1991) have set up empirical linear relationships between P-wave velocity and clay content from laboratory measurements. Marion *et al.* (1992) proposed a comprehensive model which simulated the effect of clay content on both porosity and velocity but the model was not readily applicable to formation evaluation since it required the P- and S-wave velocities of both the clean sands and ‘pure’ shales at elevated pressures (in addition to porosities). Marion *et al.* (1992) assume that the **porosity–velocity relationship for shaly sands jumps from Gassmann’s (1951) law to Reuss’ (1929) law once the shale volume exceeds the original clean sand porosity**. On physical grounds one expects a transition from one law to the other.

In the research reported here, evidence from well-logging data shows that none of the proposed porosity–velocity models is satisfactory for interpreting the scat-

tered porosity–velocity behaviour. A relationship between the effect of clays and that of aspect ratios is proposed. This leads to the development of a clay–sand model which relates elastic wave velocities (P-wave and S-wave) to both log porosity and shale volume. Finally, applications are given to demonstrate the predictive power of the porosity–velocity model.

### Porosity–velocity relationship from well-logging data

In comparison with laboratory measurements, well logging provides us with a large quantity of data. Although logging measurements have more uncertainties and lower accuracy, they are taken in real geological conditions which are difficult and expensive to simulate in the laboratory. Logging data is therefore an important source for studying porosity–velocity relationships.

In using logging data to investigate porosity–velocity behaviour, accurate log-based estimates of porosity are needed. For this purpose estimates were obtained from resistivity and density (or neutron) logs in order to provide a cross-check on accuracy wherever possible. Appendix A describes how porosity was estimated from resistivity logs.

One can predict the sonic log from the estimated porosity using one of the porosity–velocity models (e.g. Wyllie *et al.* 1956; Raymer *et al.* 1980; Krief *et al.* 1990). For shaly formations, Xu and White (poster presented at 54th EAEG meeting, Paris, 1992) considered the effects of clays on velocities to the first order by simply evaluating the transit times of the sand–shale mixtures using the time-average equation. The complete procedure is illustrated schematically in Fig. 1. Provided the estimated porosity is accurate enough, analysis of the values of physical parameters and goodness-of-fit of the measured and predicted sonic logs is a guide to the validity of the model used.

#### Case study 1: Well A

Well 44/29-1A (hereafter called Well A) is located in the southern North Sea. The oldest rocks in the interval described are the Lower Permian Rotliegendes shale, which is firmly consolidated, well indurated and, occasionally, contains thin layers of salt. The Zechstein evaporite complex overlying the Rotliegendes shale is composed of anhydrite, halite, dolomite and limestone. This is followed by the Lower Triassic Bunter shale sequence, which is firmly compacted and, occasionally, interbedded with thin layers of limestone. The Bunter sandstone (2874–2990 m, also Lower Triassic in age) is fine to medium grained, subrounded, moderately sorted and interbedded with thin layers of shale. The Bunter sandstone sequence is overlain unconformably by a shale bed of 14 m thickness which is followed by a massive salt layer (2828–2860 m). The Lower–Middle Triassic shale sequence over the depth interval 2614–2828 m is marked by the presence of denser minerals: iron, anhydrite and dolomite. The Speeton clay formation, which unconformably

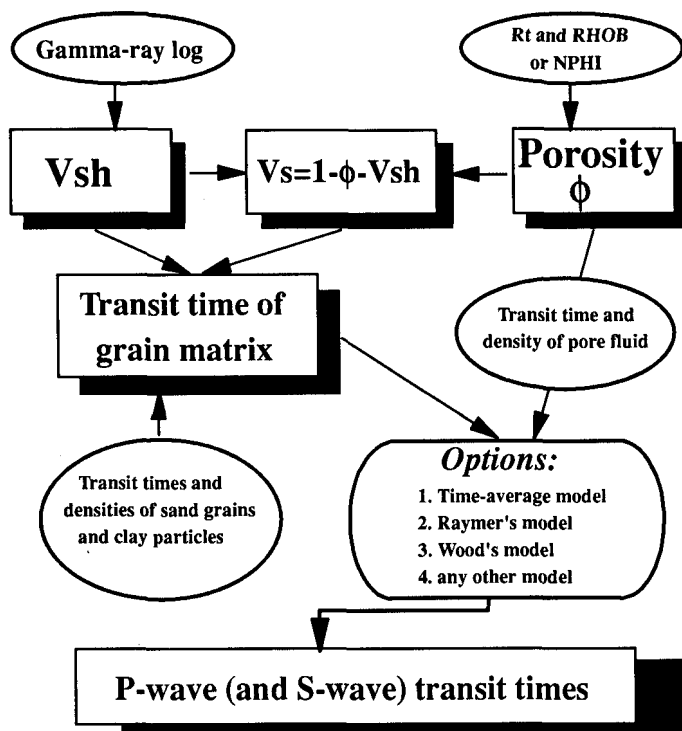


**Figure 1.** Schematic diagram of the prediction of sonic logs from other logs, where  $R_t$  denotes the resistivity log,  $RHOB$  denotes the density log, and  $NPHI$  denotes the neutron porosity log.  $\phi$  is porosity,  $V_{sh}$  is the dimensionless shale volume and  $V_s$  is the dimensionless sand volume.

overlies the shale sequence, contains disseminated carbonaceous matter, associated with a high gamma-ray count. Above the Speeton clay formation is the Upper Cretaceous Chalk sequence with a total thickness of more than 1000 m.

A density log is available over the depth interval 1400–3474 m and provides a second estimate for porosity. Figure 2 shows the gamma-ray, resistivity, density and two porosity logs and, in panel 5, the measured sonic and the pseudosonic log predicted using the time-average equation. The gamma-ray log in panel 1 was used as a clay indicator. There are two resistivity logs (ILD and ILM) available over this depth interval. The oil-based mud is very resistive and ILD was therefore used as a measure of the formation resistivity  $R_t$ . Panel 4 shows two porosity logs: PORO1, estimated from the resistivity log, and PORO2, estimated from the density log, demonstrating a good agreement between the two porosities. The composite log indicates that there are some denser minerals such as iron, anhydrite and dolomite in the interval 2500–2770 m which explains the separation of the two porosity logs there. A value of  $0.06 \Omega \text{ m}$  for  $R_w$  at a reference depth 1219 m (assuming that  $R_w$  varies with depth due to temperature) was obtained by forcing

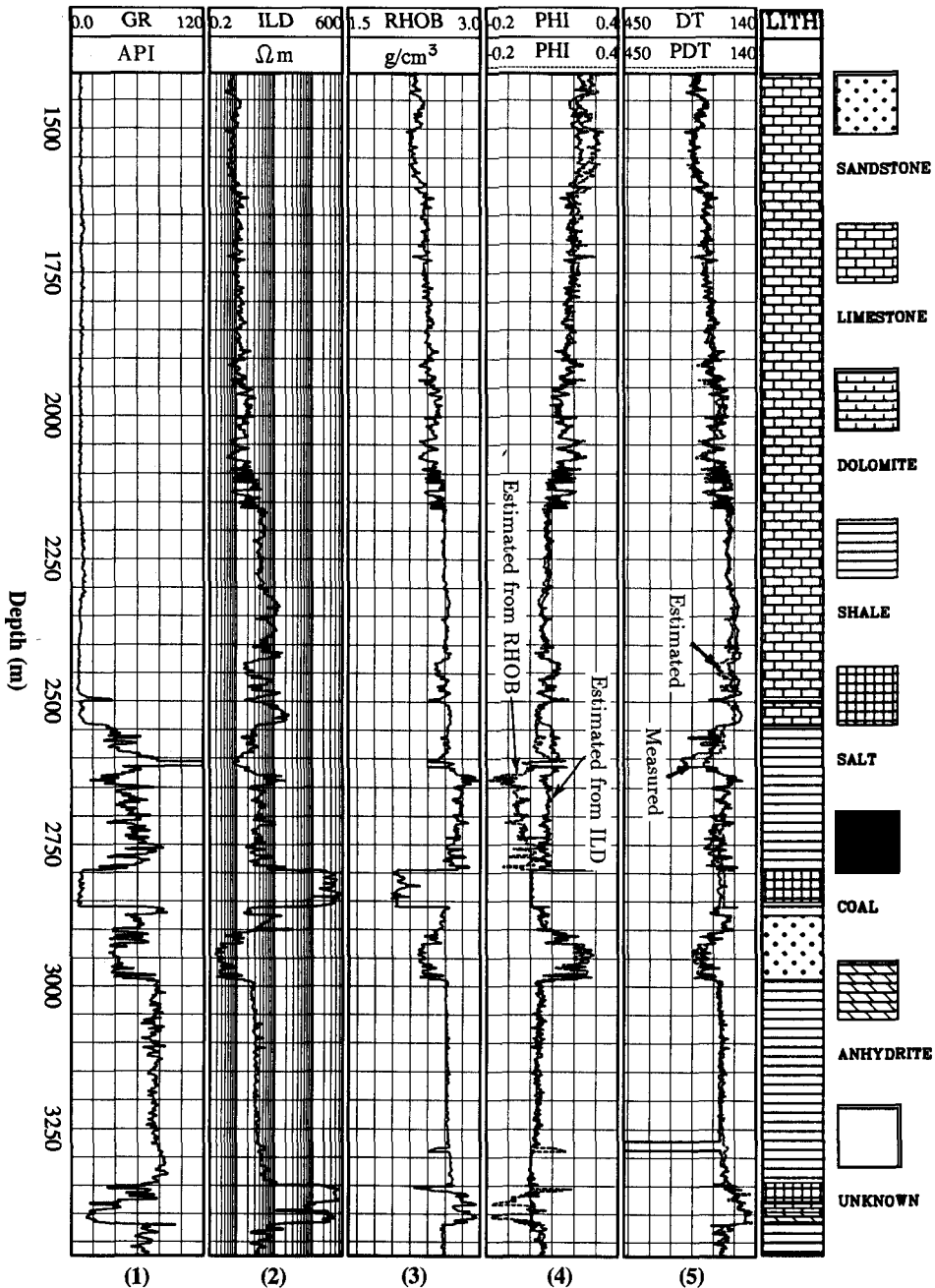


**Figure 2.** Comparison of the sonic log (DT) and the predicted sonic log (PDT) for Well A. Wyllie's time average model was used in velocity prediction. The normalized rms error for the fit is 0.057.

the two porosity logs into agreement. We took a simple average of the two porosities as the porosity used for velocity prediction except over two depth intervals (2500–2770 m and 3250–3290 m) where the porosity estimated from the density log is obviously wrong and the porosity estimated from the resistivity was therefore used.

In this case study, the Wyllie *et al.* (1956) time-average model was employed to predict P-wave transit times. Parameters for the density and P- and S-wave transit times of the different lithologies are listed in Table 1 (hereafter these values are applied to all modelling if not specifically mentioned). The normalized rms error calculated from the measured (DT) and predicted (PDT) sonic logs shown in panel 5 is 0.057, which indicates that the time-average model works reasonably well in this case.

### Case study 2: Well B

Another wireline data set with a density log available over a large depth interval was provided by Mobil North Sea. Hereafter we call this well, Well B. Although the logs are noisy, they provide us with data from rocks that range from poorly consolidated to well consolidated. The sequence starts with the Lower Triassic claystone (below 1344 m), which is light grey to grey in colour and interbedded with thin layers of limestone. This is overlain by the Kimmeridge clay formation (1036–1344 m, Upper Jurassic in age) which is mostly dark grey to black in colour with carbonaceous matter. It is medium hard, calcareous and interbedded with siltstones and thin layers of limestone. The Spilsby sandstone (906–1036 m), which uncomfortably overlies the Kimmeridge clay formation, is white to light grey in colour, fine grained and well sorted with calcareous and siliceous cement. The Lower Cretaceous Speeton clay formation (457–906 m) above the Spilsby sandstone consists mainly of claystones, which are mostly soft to firm, sticky and calcareous to non-calcareous with carbonaceous particles. Other lithologies within the Speeton clay formation are (1) unconsolidated sandstones (fine to medium grained, angular to subround, poorly sorted), (2) siltstones (medium hard, non-calcareous with carbonaceous particles) and (3) thin layers of limestone (hard to very hard, brittle, blocky and dolomitic in parts).

**Table 1.** Transit times and density for modelled rock types.

lithology	$T_p(\mu\text{s/m})$	$T_s(\mu\text{s/m})$	density ( $\text{kg/m}^3$ )
sandstone	170	260	2680
limestone	161	311	2710
shale	230 <sup>a</sup>	394	2600
salt	220	348	2000
brine	623		1100

<sup>a</sup> 262 for application of the Wyllie equation to Well A.

Figure 3 shows the resistivity log (ILD), density log (RHOB), calliper log and two porosity logs, PORO1 and PORO2, again evaluated from the resistivity and density logs. The agreement between the two porosity logs is not as satisfactory as that for Well A. The large difference between them over the depth interval 457–850 m can be attributed to the lowering of density estimates by wash-outs, in poorly consolidated rocks, that are visible on the calliper log. The two porosity logs show better agreement where the borehole is not much enlarged. A large gap between PORO1 and PORO2 around 670 m depth comes from an obvious error in the density log. PORO1 remains to the left of PORO2 at depths shallower than 850 m because underestimation of density results in overestimation of porosity. It has also been found that resistivity logs tend to overestimate porosity over sandstone intervals, 860–1020 m in this example. This may be explained by the larger inter-connectivity of sands in comparison with shales, implying that different values for the cementation factor should be assigned for sands and shales. We simply average the two porosity measurements over this depth interval in order to reduce the porosity errors.

The porosity log finally used in velocity prediction is shown in panel 3 of Fig. 4. Panel 4 shows the measured sonic log (DT) and the pseudosonic logs predicted using both the time-average equation (PDT1) and Wood's (1941) suspension model (PDT2). It can be seen that neither of these models is satisfactory over the whole depth interval (the normalized rms error is 0.23 for the Wyllie *et al.* (1956) time-average equation and 0.25 for Wood's (1941) suspension model). Basically, the measured transit times fall between PDT1 and PDT2. It appears that the time-average model provides good results for sand layers (860–1020 m), whereas the results from Wood's (1941) model tend to approach the measured transit times for shales. This implies that the porosity–velocity relationship for sands is fundamentally different from that for shales. The same behaviour has also been observed in the laboratory by Marion *et al.* (1992). The measurements of both porosities and P-wave velocities of shaly sands and sandy shales are very scattered but lie between Wood's (1941) model and the Wyllie *et al.* (1956) time-average model (Fig. 5).

#### *Some key points from the case studies*

All the evidence above suggests that it is clays that introduce scatter into the porosity–velocity relationship. Two points of particular note are that the time-average equation works well in the first case but not in the second and that the porosity–velocity relationship for sands is notably different from that for unconsolidated shales. These observations lead us to look for another factor, besides porosity, which controls the elastic behaviour of porous rocks.

Let us first examine the assumptions of the time-average model. The model is valid only for rocks that are (1) well cemented and consolidated and (2) under high effective pressure (Jordan and Campbell 1986). Now cementation implies that small gaps and cracks are filled by cements, leaving large pores with large aspect ratios open. Also the aspect ratios of pores in real rock are not simply distributed

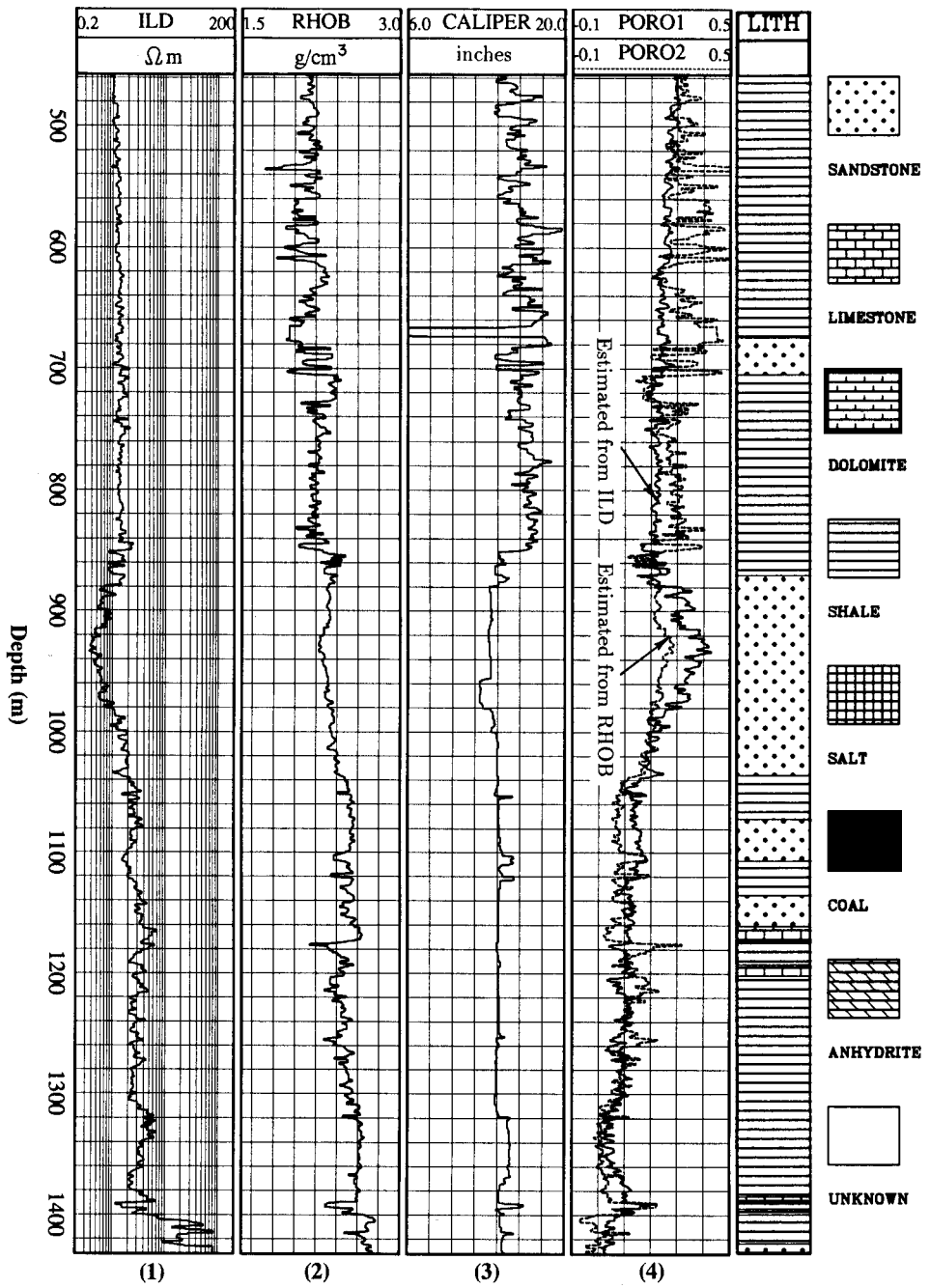


**Figure 3.** Comparison of the porosity logs for Well B: PORO1, estimated from resistivity log (ILD), and PORO2, estimated from the density log (RHOB).



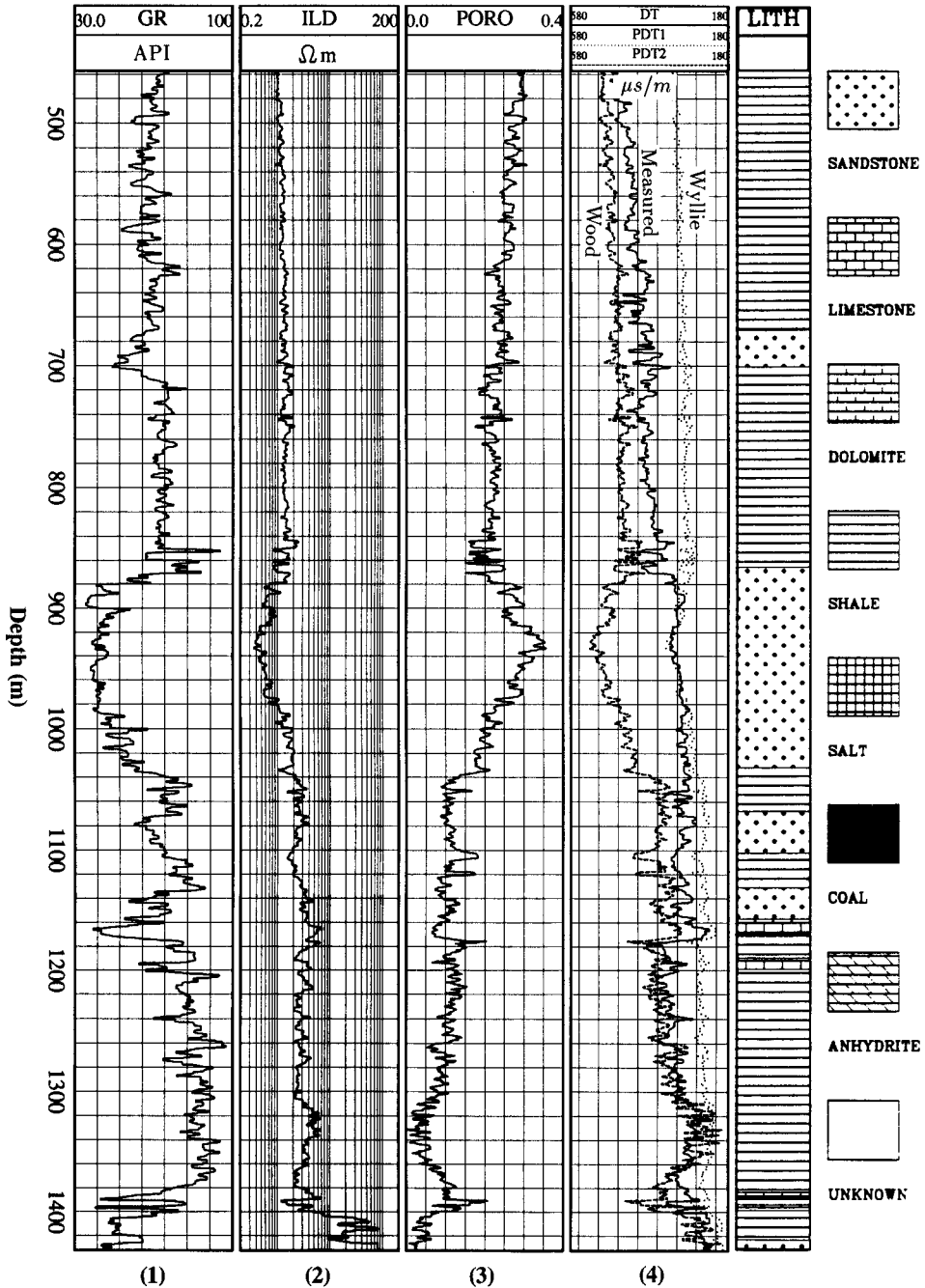


**Figure 4.** Comparison of sonic log (DT) and the predicted sonic logs for Well B: PDT1 (using the time-average equation with a normalized rms error of 0.23) and PDT2 (using Wood's suspension equation with a normalized rms error of 0.25).

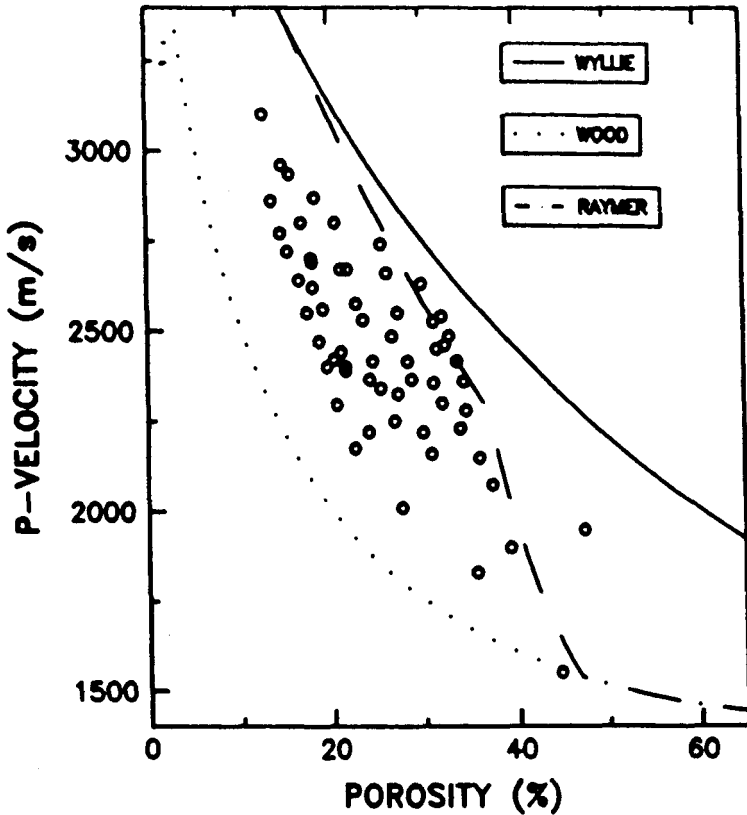


**Figure 5.** Relationships between the measured porosities and P-wave velocities for synthetic shaly sands and sandy shales and comparison with conventional porosity-velocity models. After Marion *et al.* (1992).

according to some unimodal distribution, but rather are concentrated around particular aspect ratios. Consequently high effective pressure closes pores with very small aspect ratios like microcracks, leaving large aspect ratio pores open. In effect the mean aspect ratio can increase with confining pressure. There is a hint, therefore, that it is pore geometry that decides the validity of the time-average model.

The most significant aspect of clays could be the particular shape of clay particles which, in turn, controls the geometrical behaviour of the pore spaces associated with them. Flaky clay particles tend to form pores with small aspect ratios. This explains why compaction affects shales much more than any other sedimentary rock. In terms of the Kuster and Toksöz theory (1974), it is expected that clays would affect the relationship between velocity and porosity. This could be just as significant as the effect of clays on porosity.

Eastwood and Castagna (1983) also concluded that the aspect ratio of pores plays as significant a role as porosity in velocity determination, especially when the

aspect ratio is less than 0.05. From the discussion above, it appears that it is the aspect ratio, in addition to porosity, that is significant in controlling the elastic behaviour of sand and clay mixtures. This speculation is tested by the numerical results and the tests of sonic log prediction shown below.

The large burial depth of the shale formations (all below 2500 m) gives the clue to the reason why the Wyllie *et al.* (1956) time-average equation worked well in the first case study. Clay particles create compliant pores with small aspect ratios, most of which are closed by the lithostatic pressure at such depths if the shales are not overpressured (Toksöz, Cheng and Timur 1976). In this case clays contribute only to the elastic properties of the grain matrix and this effect can be simulated by the time-average model. In the second case study, the shales are poorly compacted and poorly consolidated due to the low lithostatic pressure. Pores associated with clay particles are still open under such pressures. In this case, clays affect not only the elastic properties of the grain matrix but also the porosity-velocity relationship which no longer obeys the time-average model of Wyllie *et al.* (1956).

### The Kuster-Toksöz model and effective medium theory

Many factors, such as porosity, pore geometry, cementation, fluid relaxation, clays, pressure and frequency, influence elastic wave propagation in porous rocks. If some factors are simply the by-products of others, the number of independent factors can be reduced. Our clay-sand mixture model postulates two major factors, porosity and aspect ratio. Then the effects of clays, cementation and pressure can possibly be subsumed by pore aspect ratio as follows.

1. Clay particles create pores with very small aspect ratios, as discussed in the previous section.
2. Cementation reduces the number of gaps with small aspect ratios. Less cemented rocks have more gaps than cemented rocks.
3. Effective pressure controls the closure of cracks (gaps with low aspect ratios).

Many theoretical studies confirm the effect of pore aspect ratios on elastic wave velocities (e.g. Eshelby 1957; Wu 1966; Nur 1971; Kuster and Toksöz 1974; O'Connell and Budiansky 1974; Hudson 1981; Nishizawa 1982). In a series of papers (e.g. Kuster and Toksöz 1974; Cheng and Toksöz 1979; Toksöz *et al.* 1976), Toksöz and his co-authors developed a model for a two-phase medium which relates both porosity and pore aspect ratios to the P- and S-wave velocities. One major concern in using the Kuster and Toksöz (1974) theory is the assumption that pore or crack concentration must be dilute, i.e.

$$\frac{\phi}{\alpha} \ll 1. \quad (1)$$

In other words, the theory is valid only for rocks containing pores with a porosity  $\phi$  much less than pore aspect ratio  $\alpha$ . This limitation arises from ignoring the inter-

actions between pores. Several efforts have been made to consider the interactions between pores. These led, for example, to the so-called self-consistent theory (e.g. O'Connell and Budiansky 1974) which was later found to overestimate the effect of the interactions, almost doubling the true effect. A new self-consistent scheme, the effective medium theory, was then employed by many authors to deal with the interaction problem (e.g. Nishizawa 1982). Zimmerman (1984) reported that the effective medium theory provides results closer to the experimental data than other theories.

The general idea of effective medium theory is as follows. The total number of pores or cracks can be divided into  $N$  sets. The pore concentration for each set is so small that the assumption of a dilute pore concentration is valid. In this case, the Kuster and Toksöz (1974) theory can be applied to calculate the effective elastic properties of the medium after inserting a dilute concentration of pores without any problem. Another set of pores is introduced into the effective medium in a similar way, and the effective elastic constants are then updated. This procedure is repeated until the total pore concentration is reached.

In general, the larger  $N$  is, the more accurate are the results. Figure 6 shows P-wave transit times for both saturated and dry rock as a function of the number of sets of pores. Both porosity and aspect ratio are assumed to be 0.1 in this numerical study, corresponding to a  $\phi/\alpha$  ratio of 1. Two conclusions can be drawn from this diagram. Firstly, ignoring the interactions between pores gives overestimates of

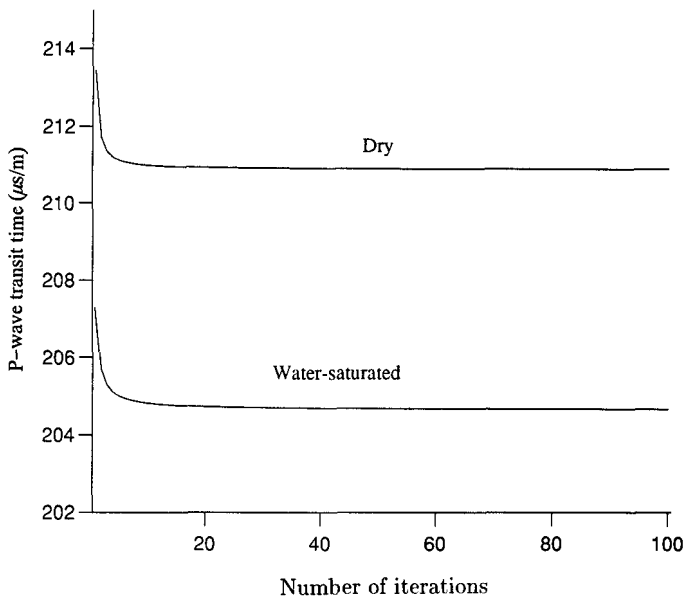


**Figure 6.** P-wave transit times approximated using the Toksöz model and effective medium theory as a function of the number of iterations.  $\phi/\alpha = 1$ .

transit times (underestimating velocities). Secondly, the estimated transit times vary dramatically with  $N$  initially and remain fairly constant after  $N$  exceeds 10 in this particular example. This implies that the Kuster and Toksöz (1974) theory provides fairly accurate velocity approximations (Nishizawa 1982; Zimmerman 1984) for rocks having  $\phi/\alpha$  less than 0.1. This criterion is a useful compromise between computing time and accuracy which avoids slowing down practical applications of the model with heavy computations due to the use of a large  $N$ .

A numerical example is presented here to show the effect of the pore aspect ratio on the porosity–velocity relationship and to compare the Toksöz model with other standard models. The matrix is given a P-wave transit time of  $171 \mu\text{s/m}$ , an S-wave transit time of  $256 \mu\text{s/m}$  and a density of  $2650 \text{ kg/m}^3$ . The rock is assumed to be 100% saturated with brine having a P-wave transit time of  $623 \mu\text{s/m}$  and a density of  $1100 \text{ kg/m}^3$ .  $\alpha$  varies from 0.01 to 0.15 and  $\phi$  from 0.01 to 0.4. The number of iterations  $N$  was 800 which guarantees accurate results for all cases.

Figure 7 shows the numerical results and comparisons with Wood's (1941) suspension model, the Wyllie *et al.* (1956) time-average model and the model of Raymer *et al.* (1980) for hard formations. The results demonstrate that pores with large aspect ratios are much stiffer than those with small aspect ratios, to a degree sufficient to affect velocity significantly. This is the basis for stating that it is the

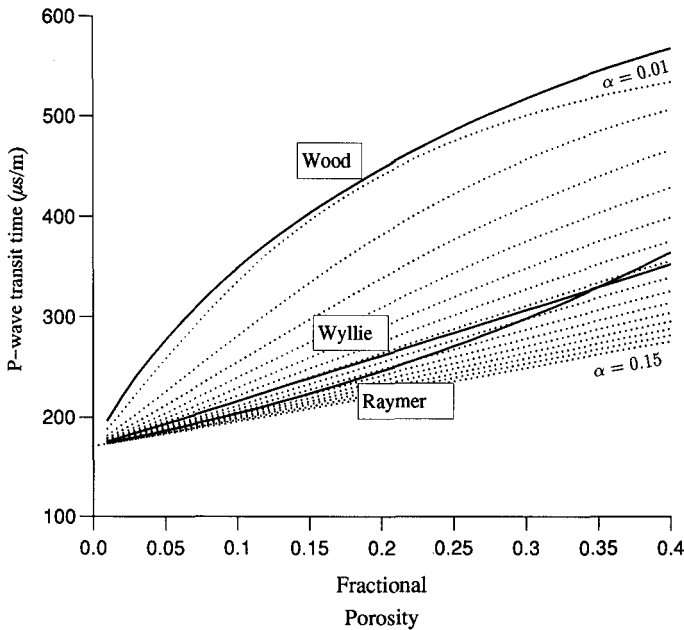


**Figure 7.** Transit times (dotted lines) estimated using the Toksöz model and effective medium theory as a function of porosity and pore aspect ratio (aspect ratio varies from 0.01 in 0.01 steps to 0.15) and comparison with other published models.

pore aspect ratio that puts scatter into the porosity-velocity relationship. Comparison of the time-average model with these results suggests that the time-average model is valid for rocks containing pores with the mean aspect ratio roughly equal to 0.07 rather than rounded pores. Wood's (1941) suspension model agrees with the Toksöz model for an aspect ratio slightly less than 0.01. The suspension model provides an upper bound for transit times because suspension really means no stiffness of the pores. According to Figs 4 and 5, the measured transit times are always smaller than those predicted from Wood's (1941) model.

### A new clay-sand mixture model

The new velocity model for clay-sand mixtures has been developed from the Kuster-Toksöz (1974) model, supplemented by effective medium theory, and Gassmann's (1951) model. The key part of the model is the hypothesis that aspect ratios for sand-related pores are significantly different from those for clay-related pores. The sand-related pores have a mean aspect ratio  $\alpha_s$  and the clay-related pores a mean aspect ratio  $\alpha_c$ . The sum of the pore volumes related to sand grains,  $\phi_s$ , and those related to clays,  $\phi_c$ , is equal to the total pore space of the mixture, i.e.

$$\phi = \phi_s + \phi_c. \quad (2)$$

There is no information on how much pore space is associated with sands and how much with clay. To a first-order approximation, it is assumed that  $\phi_s$  and  $\phi_c$  are directly proportional to sand grain volume and clay content. In practice log analysis gives shale volume not clay content.  $\phi_s$  and  $\phi_c$  are therefore approximated by the following equations:

$$\phi_s = V_s \frac{\phi}{1 - \phi} \quad (3)$$

and

$$\phi_c = V_{sh} \frac{\phi}{1 - \phi}, \quad (4)$$

where  $\phi$  is the total effective porosity as determined from a porosity log or a resistivity log (Xu and White 1992, as above).  $V_{sh}$  denotes the dimensionless shale volume, which can be determined from one of the shale indicators or a combination of them, and  $V_s$  is the dimensionless sand volume, as estimated from

$$V_s = 1 - \phi - V_{sh}. \quad (5)$$

In order to evaluate elastic wave velocities of shaly sands or sandy shales, the P- and S-wave transit times of the mixture of the sand grains and clay particles are evaluated using the time-average equations,

$$T_m^p = (1 - V_{sh}') T_g^p + V_{sh}' T_{sh}^p \quad (6)$$

and

$$T_m^s = (1 - V'_{sh})T_g^s + V'_{sh} T_{sh}^s. \quad (7)$$

The density is found from

$$\rho_m = (1 - V'_{sh})\rho_g + V'_{sh} \rho_{sh}. \quad (8)$$

$T_g^p$ ,  $T_{sh}^p$  and  $T_m^p$  are the P-wave transit times of the sand grains, clay minerals and the mixture of them, respectively.  $T_g^s$ ,  $T_{sh}^s$  and  $T_m^s$  are the corresponding S-wave transit times and  $\rho_g$ ,  $\rho_{sh}$  and  $\rho_m$  are the corresponding densities.  $V'_{sh}$  is the shale volume normalized by the volume of solid matrix and is given by

$$V'_{sh} = \frac{V_{sh}}{1 - \phi}. \quad (9)$$

Elastic bulk and shear moduli of the mixture of sand grains and clay minerals are calculated from the P- and S-wave transit times and the density of each component.

The next step is to evaluate the elastic properties of the dry frame using the Kuster and Toksöz theory (1974):

$$K_d - K_m = \frac{1}{3}(K' - K_m) \frac{3K_d + 4\mu_m}{3K_m + 4\mu_m} \sum_{l=s,c} \phi_l T_{ijj}(\alpha_l), \quad (10)$$

$$\mu_d - \mu_m = \frac{(\mu' - \mu_m)}{5} \frac{6\mu_d(K_m + 2\mu_m) + \mu_m(9K_m + 8\mu_m)}{5\mu_m(3K_m + 4\mu_m)} \sum_{l=s,c} \phi_l F(\alpha_l), \quad (11)$$

where

$$F(\alpha_l) = T_{ijj}(\alpha_l) - \frac{T_{ijj}(\alpha_l)}{3}. \quad (12)$$

Here  $K_d$ ,  $K_m$  and  $K'$  are the bulk moduli of the dry frame, the mixture and the fluid, respectively;  $\mu_d$ ,  $\mu_m$  and  $\mu'$  are the corresponding shear moduli. In order to derive the moduli of the dry matrix frame (empty pores),  $K'$  and  $\mu'$  are assumed to be zero in this stage. The scalars  $T_{ijj}$  and  $T_{ijj}$  are functions of the aspect ratio (the ratio of short semi-axis to long semi-axis) and the properties of the matrix and the fluid enclosed and are given in Appendix B.

Finally the Gassmann (1951) model is used to simulate the effect of fluid relaxation. White (1965) formulated the Gassmann model for the compressional velocity  $v_p$  as

$$v_p = \left\{ \frac{1}{\rho_b} \left[ K_d + \frac{4}{3}\mu_d + \frac{(1 - C_m/C_d)^2}{C_m(1 - \phi) + C_f\phi - C_m^2/C_d} \right] \right\}^{1/2}, \quad (13)$$

where  $\rho_b = \rho_m(1 - \phi) + \rho_f\phi$ ,  $K_d$  and  $\mu_d$  are the bulk and shear moduli of the dry rock, and  $C_m$ ,  $C_f$  and  $C_d$  are, respectively, the grain mixture, fluid and dry rock

frame compressibilities. The shear-wave velocity  $v_s$  of the rock permeated by non-viscous fluid is simply

$$v_s = \left\{ \frac{\mu_d}{\rho_b} \right\}^{1/2}. \quad (14)$$

It is possible to calculate the elastic properties of saturated rock using only the Toksöz model. The reason for not doing so is that pores in the Toksöz model are assumed to be isolated implying that the pore fluid is only locally relaxed. We assume that the elastic properties of a dry rock with interconnected pores are essentially equal to those of the same dry rock with isolated pores. Therefore we use the Toksöz model to estimate the elastic properties of dry rock frame and the Gassmann (1951) model to consider the effect of fluid relaxation.

The model requires knowledge of the aspect ratios of both clay-related pores and sand-related pores in order to predict the relationships between porosity, clay content and wave velocities. Although we know that the mean aspect ratio for sand-related pores is markedly larger than that for clay-related pores, we need to assign magnitudes to them. Direct measurement from thin sections can give some idea of their magnitudes but the aspect ratio required by our model is not a simple mean but the effective mean with respect to the elastic compliance of the pores, i.e. a pore compliance index. There is no clear way of determining this index directly and it has to be estimated indirectly by matching the model with P- and S-wave velocities, either from laboratory measurements or from logging data. We therefore use the goodness-of-fit between measurements and predictions of the model to investigate its validity. None the less, mean aspect ratios found from fitting the model should be of the same order as directly measured ratios.

## Applications

### *Predicting sonic logs from other logs*

The initial objective of this research was the quality control and prediction of sonic logs from other logs over large depth intervals for the purpose of constructing accurate synthetic seismograms. Comparison of a measured sonic log with the log predicted from other logs, such as resistivity, gamma-ray and density logs, acts as a check on the consistency of the measurements and, if successful, can provide replacement values for a P-wave sonic in wash-out zones and even complete S-wave logs. The basic idea is first to evaluate porosity and shale volume from resistivity, gamma-ray and density (if available) logs using the improved model of Xu and White (1992, as above). Special lithologies such as salt and coal can also be identified, depending on the logs available. Then the P-wave and S-wave transit times in clay-sand mixtures can be calculated using the model developed above.

Our first application is the prediction of the P-wave sonic log from Well B which was discussed above. There it was found that neither the time-average nor the Wood (1941) model could predict this particular log, the poor predictability being



attributed to the effect of clays. An empirical equation of the type derived from laboratory measurements by Han *et al.* (1986) was then employed in order to account for the effect of clays on the transit-time prediction. Figure 8 (panel 3) shows the best fit between the measured sonic log (DT) and the predicted sonic log (PDT) using an equation of the same form as that given by Han *et al.* (1986). The calculated normalized rms error is 0.12, an obvious improvement in comparison with Fig. 4. However, the predicted transit times are underestimated at shallower depths (about 457–700 m) and overestimated deeper (about 1260–1400 m). Some large differences occur at depths around 860 m. Figure 8 (panel 4) shows the comparison of the measured sonic log (DT) and the predicted sonic log (PDT) using the clay–sand model developed above. The same model parameters, apart from the aspect ratios, and the same log-derived quantities as those used in Fig. 4 were used here. The best-fit aspect ratio for grain-related pores was 0.12 and that for clay-related pores was 0.02. In comparison with Fig. 4 and panel 3 of Fig. 8, the clay–sand mixture model has yielded a further improvement (normalized rms error 0.07) in the prediction of the sonic log.

Because of the significant influence of clays on velocities, the accuracy of the shale volume estimation becomes important in our velocity prediction. For example, the large local differences between our predictions and the measurements at depths around 860 m are probably caused by organic matter, which normally has very high radioactivity. It would therefore be helpful to use other shale indicators such as SP, NGS (natural gamma-ray spectra), if available, as well as gamma-ray logs in order to obtain more accurate estimates of shale volume.

It was shown above that the time-average model gave reasonable results for Well A over a large depth interval. Results for the new model are shown in Fig. 9: the gamma-ray log (panel 1), two porosity logs (panel 2) and the comparison between the measured sonic log (DT) and two sonic logs (PDT) predicted by the new model (panels 3 and 4). The difference between panels 3 and 4 is that the former employs an aspect ratio of 0.12 for carbonate-related pores in its predictions whereas the latter employs an aspect ratio of 0.10. Both panels employ 0.02 for the aspect ratio of clay-related pores and 0.12 for that of sand-related pores. The same porosity estimates as those of Fig. 2 were applied throughout. In comparison with Fig. 2, the following points can be noted.

1. There is no obvious improvement over the time-average model; the normalized rms errors are 0.053 for panel 3 and 0.049 for panel 4. It is to be expected that, at large burial depths of shale formations, say beyond 2500 m provided the pore fluid is not overpressured, lithostatic pressure closes most clay-related pores. If so, the effect of clay on velocity can be approximated by the time-average equation and there will be little variation with depth.
2. A mean aspect ratio of 0.10 predicts velocities in carbonates (the log above 2500 m) better than 0.12. Tatham (1982) and Tao and King (1993) also report that aspect ratios in carbonates are smaller than in sandstones.

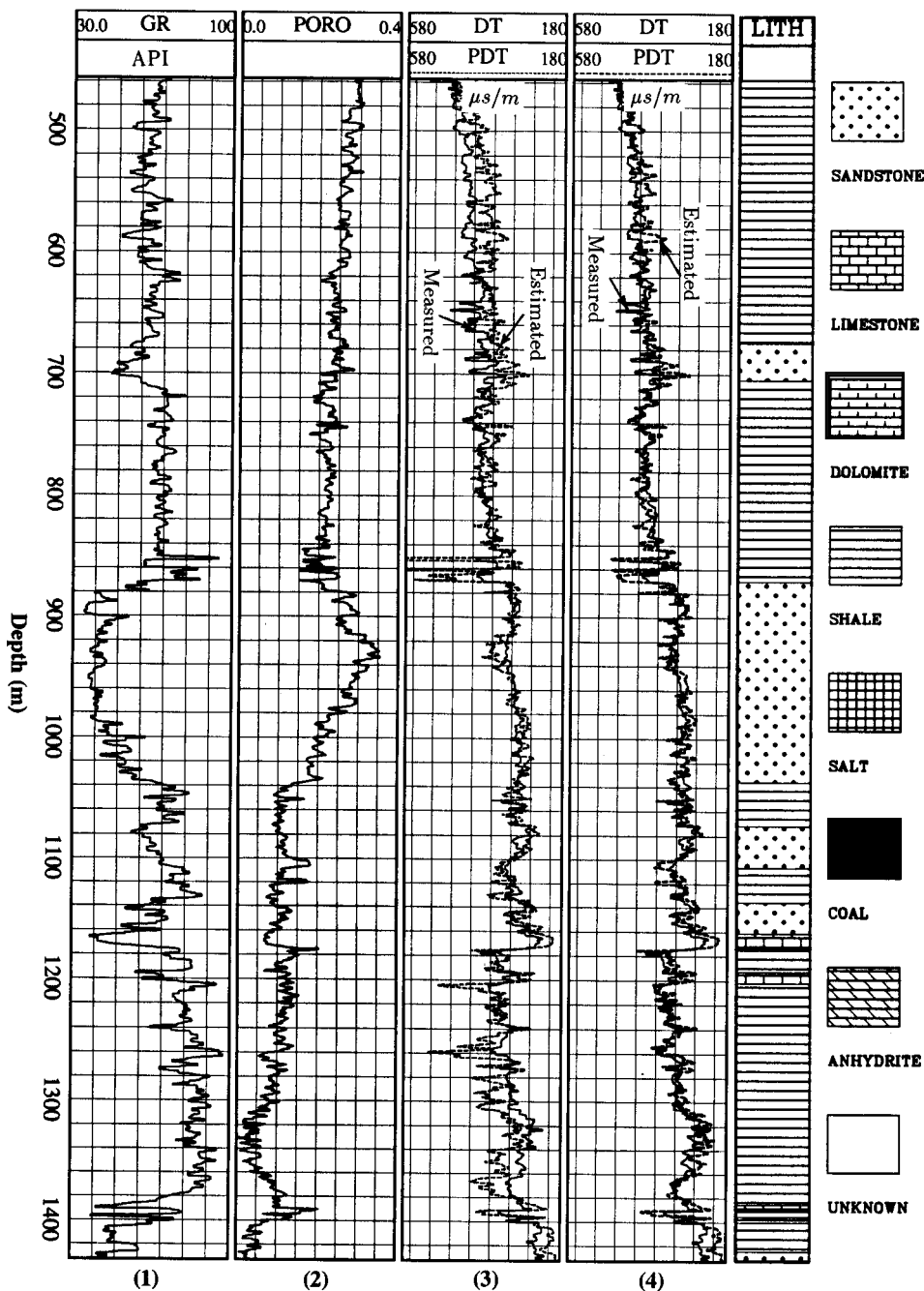


**Figure 8.** Comparison of the sonic log (DT) and the predicted sonic logs (PDT) for Well B: (panel 3) using a best-fit equation of the same form as the empirical model proposed by Han *et al.* (1986) and (panel 4) using the new clay-sand mixture model. The calculated rms error is 0.12 for panel 3 and 0.07 for panel 4, respectively.

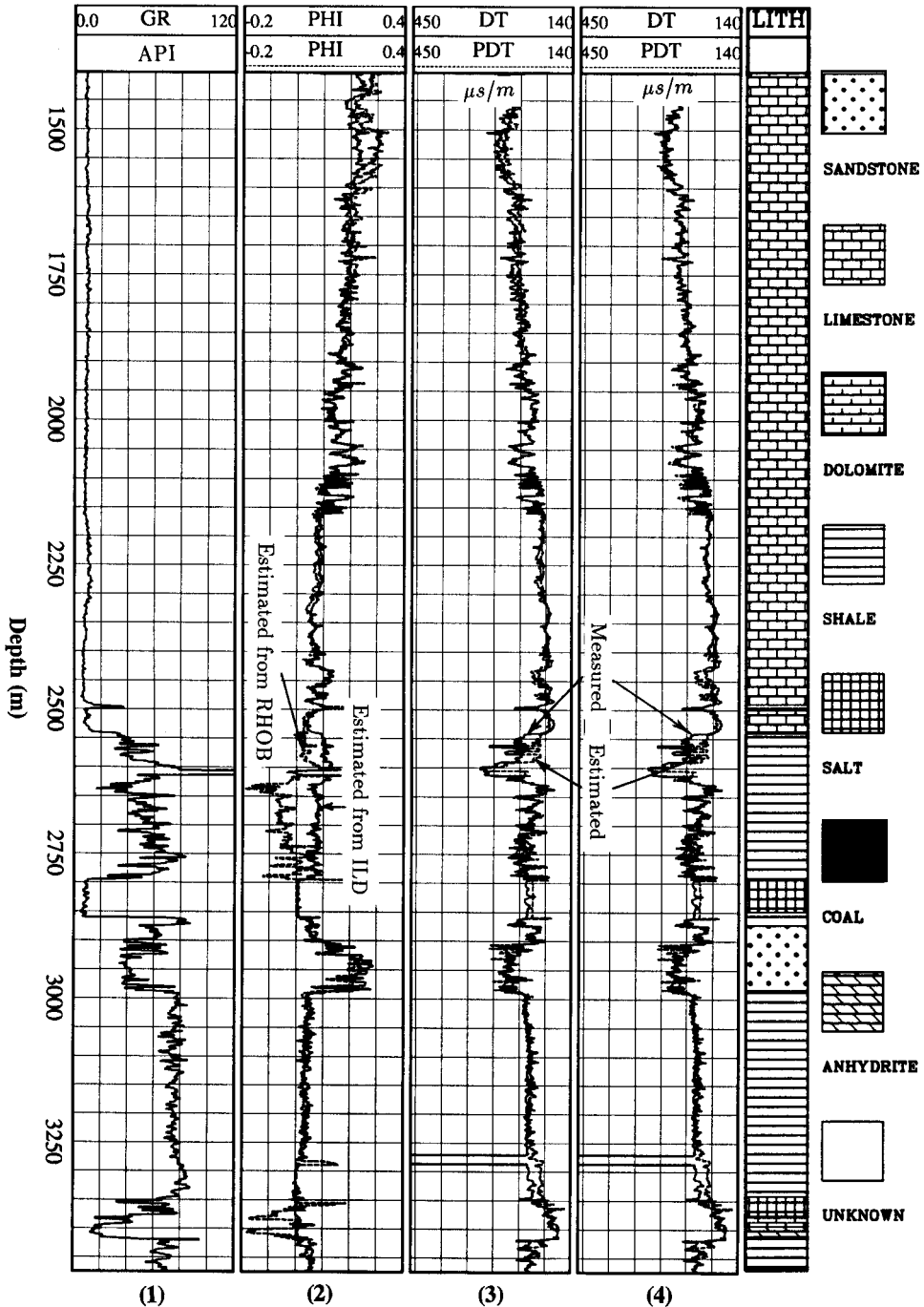


**Figure 9.** Comparison of the sonic log (DT) and the predicted sonic log (PDT) for Well A using the new clay-sand mixture model. Panel 3: assuming a mean aspect ratio of 0.02 for clay-related pores and 0.12 for the rest; panel 4: assuming a means aspect ratio of 0.02, 0.12 and 0.1 for clay-, sand- and carbonate-related pores. The calculated rms error is 0.053 for panel 3 and 0.049 for panel 4.

### *Application to laboratory measurements*

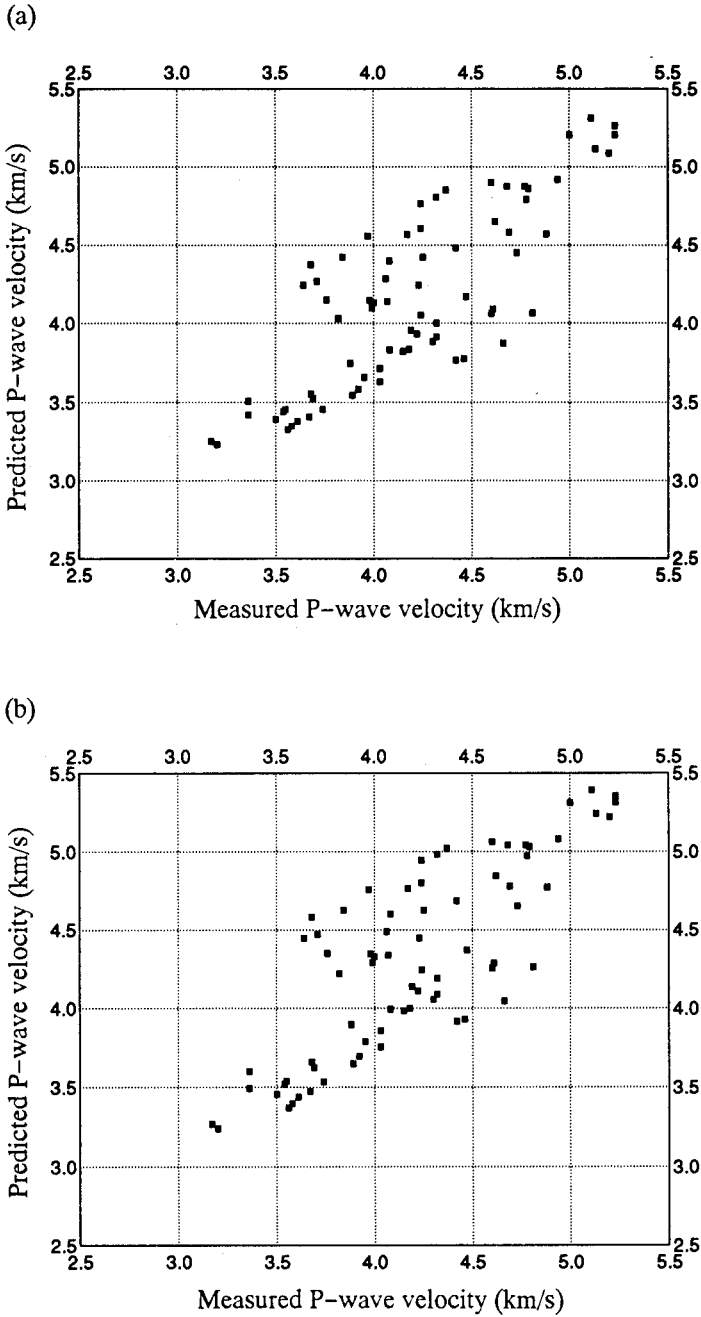
Han *et al.* (1986) carried out a comprehensive laboratory study of the effect of clay on P- and S-wave velocities. The authors measured porosity, clay content, and the P- and S-wave velocities of 75 sandstone samples at elevated confining pressures with a constant pore pressure of 1 MPa and found that the P- and S-wave velocities could be expressed as linear functions of porosity and clay content. The constants in these empirical relationships varied with confining pressure.

Figure 10 shows cross-plots of the measured P-wave velocities against the P-wave velocities predicted using (a) the time-average model and (b) the Raymer *et al.* (1980) model for hard formations at a confining pressure of 40 MPa. As can be seen from the figures, the relationships between the measured and predicted velocities are highly scattered. Figure 11a shows the equivalent cross-plot using the predictions from our model; this cross-plot is indistinguishable from that obtained from the predictions of Han *et al.* (1986). The model can also predict S-wave velocities from the same parameters (for reasons of space we leave details to a subsequent paper). The cross-plot of S-wave velocities from our model in Fig. 11b shows less scatter than the predictions of Han *et al.* (1986). The improvement of Fig. 11a over Fig. 10 is significant, implying that much of the scatter in Fig. 10 can be attributed to variations in pore geometry.

The aspect ratios applied in the modelling were 0.15 for sand-related pores and 0.04 for clay-related pores, which are both higher than those applied in the sonic log prediction. This may be a consequence of the poor consolidation of the rocks at Well B compared with the sandstone samples tested by Han *et al.* (1986). More pores or gaps with small aspect ratios are present in less consolidated formations. The distribution of pore aspect ratios is generally not unimodal but multimodal, being concentrated on particular aspect ratios that may relate to grain sorting, transportation, cementation, etc. This behaviour complicates the effects of pressure on elastic velocities. In general, all aspect ratios must decrease with confining pressure, but like microcracks, pores with very small aspect ratios are more sensitive to confining pressure than other pores. The closure of those pores effectively increases the mean aspect ratio of the remaining pores.

Velocity dispersion (the effect of frequency) and errors in evaluating shale volume give rise to other uncertainties in comparing results obtained in the laboratory with those from well-logging data. Shale volume estimated from X-ray counts is generally higher than that from gamma-ray logs, although there exists a linear trend between them (Rider 1986). The clay-sand model tends to compensate an underestimated shale volume with a decreased aspect ratio  $\alpha_c$ . Thus the difference between the aspect ratio of the clay-related pores obtained in the laboratory and that from logging is in the direction expected from evaluating shale volumes from gamma-ray logs that are not calibrated by X-ray counts.

A recent study published by Hornby, Schwartz and Hudson (1993) suggests that the mean aspect ratio for kaolinite is roughly 0.05. Although not much can be made of measurements on different rock samples, this value does show that our best-fit



**Figure 10.** Cross-plot of the measured P-wave velocity versus the predicted P-wave velocity using (a) Wyllie's (1956) time-average equation and (b) Raymer's (1980) model for hard formations. Data are taken from Han *et al.* (1986).

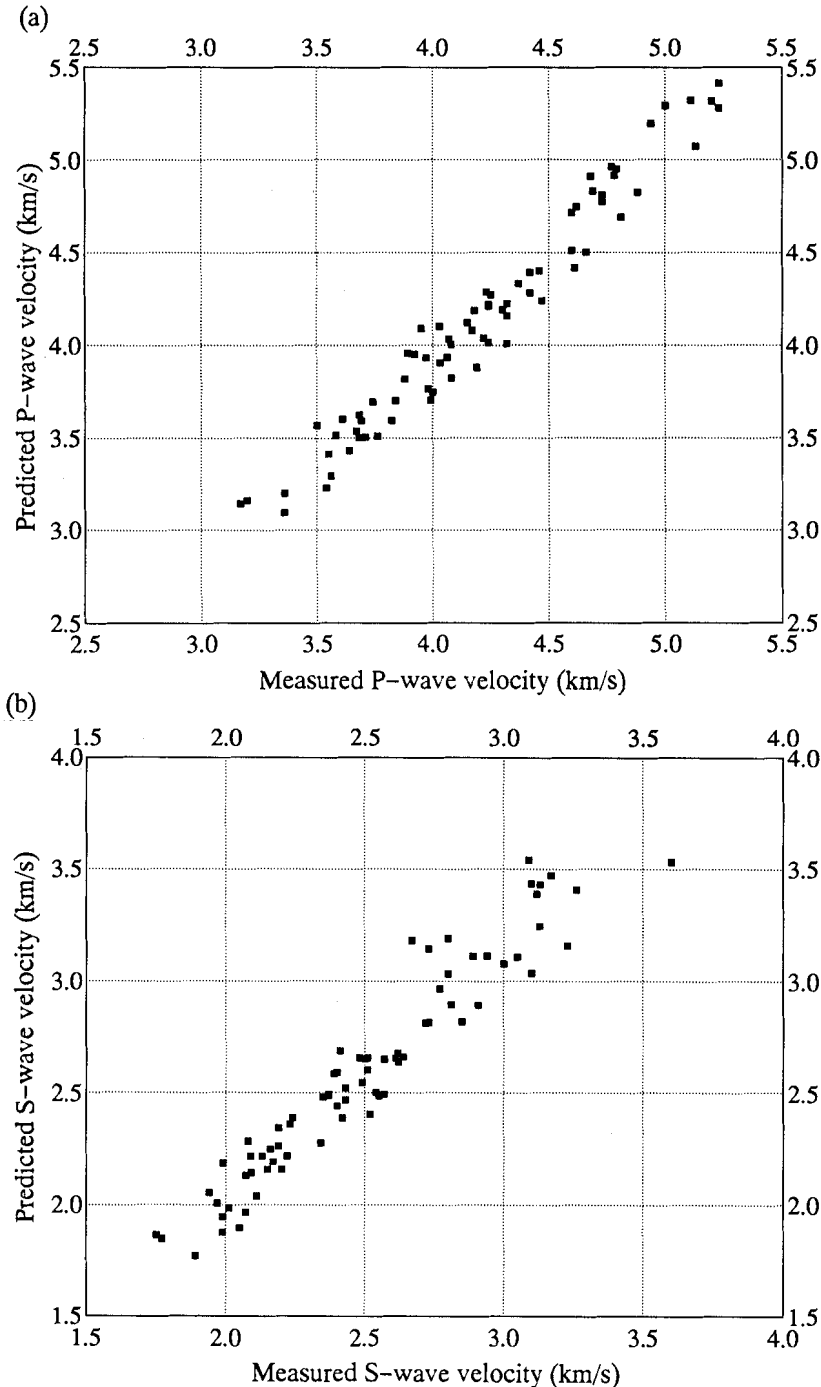


**Figure 11.** Cross-plot of the measured wave velocities versus the predicted wave velocities using the **clay-sand mixture model**. The measurements were taken at 40 MPa confining pressure and 1 MPa pore pressure by Han *et al.* (1986). (a): P-wave velocity; (b): S-wave velocity.

value ( $\alpha_c = 0.04$ ) to the laboratory measurements of Han *et al.* (1986) is of the correct order. For sand-related pores, the aspect ratios depend primarily on the geometry of the sand grains and secondarily on factors such as cementation, sorting and pressure. The mean aspect ratio for unconsolidated sands is certainly lower than that for the consolidated sandstone, assuming other conditions are the same, since unconsolidated sands are more likely to have gaps with small aspect ratios that would be closed by pressure or filled by cementation. Toksöz *et al.* (1976) showed histograms of aspect ratios determined from SEM photographs of Boise sandstone. At effective pressures, above 500 bars, the majority of the pores were concentrated at aspect ratios around 1 and 0.1, which agrees qualitatively with our best-fit values (0.12–0.15) for the mean aspect ratio for sand-related pores, on the supposition that the lower aspect ratio would dominate the pore compliance.

### More results and discussion

The successful application of the new model to both laboratory measurements and logging data is an encouraging indication of its validity. The best-fit mean aspect ratio of clay-related pores is notably smaller than that of sand-related pores. Although these aspect ratios may vary from one rock to another because of geological variations, such as grain transportation, sorting and cementation, it is postulated that these changes are small compared with the difference between  $\alpha_s$  and  $\alpha_c$ .

The model can also explain the two distinct porosity–velocity trends observed in the laboratory by Marion *et al.* (1922), one for shaly sand and the other for sandy shale (Fig. 12). Figure 13 shows the porosity–velocity relationships from our model (solid lines,  $\alpha_s = 0.15$ ,  $\alpha_c = 0.04$ ) as the clay content varies from 0% (clean sands) to 60% of the total volume. The results show that P-wave velocity is not a simple linear function of porosity and clay content. The results also match the two trends in the Marion *et al.* (1992) porosity–velocity plots. The dots in Fig. 13 demonstrate the P-wave velocity change with clay content for a sandstone with 32% original porosity. In this simulation the effect of clays on porosity was approximated using the model proposed by Marion *et al.* (1992), with a porosity of 20% for ‘pure shale’.

As can be seen from Fig. 13, clays first fill the pores and reduce porosity. The P-wave velocity at first decreases slightly with clay content, indicating the stronger influence of density than of elastic moduli at this stage. This confirms Anstey's (1991) prediction. Once the sand pores are completely packed by clay, the effect of clays on the elastic moduli of the effective medium become more important and the P-wave velocity increases with clay content. When the clay content reaches the original porosity, the effective porosity is a minimum because all pores are exactly filled by clays and their associated pores. After that, sand grains are held within the clay and porosity will increase if more clays are introduced, causing a reduction in the P-wave velocity. This prediction agrees qualitatively with the laboratory measurements of Marion *et al.* (1992) on synthetic and real shaly sandstone samples.

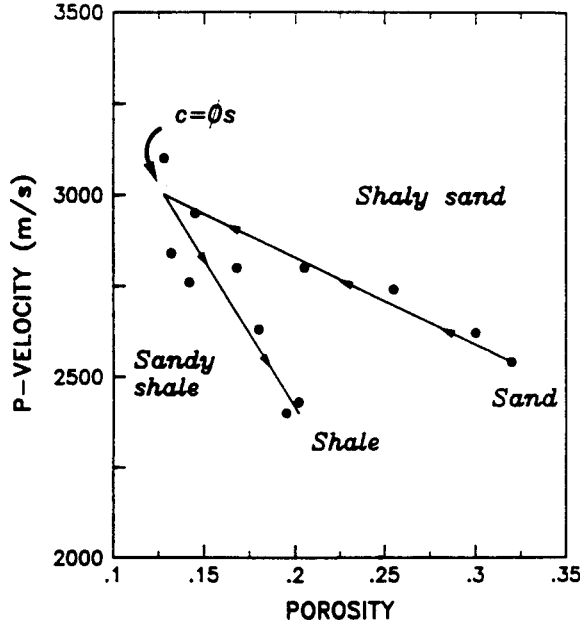


**Figure 12.** Laboratory measurement of the two porosity–velocity trends: one for shaly sand and the other for sandy shale (after Marion *et al.* 1992). Arrows indicate the direction of increasing clay content.

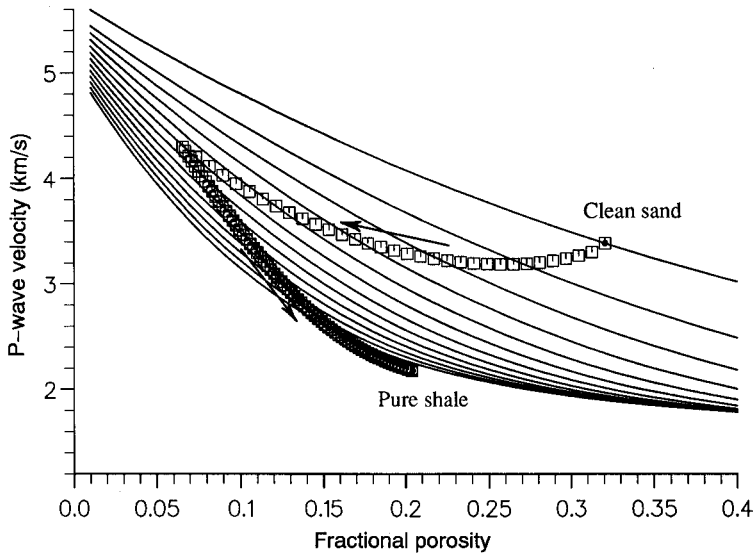


**Figure 13.** Porosity–velocity relationship as clay content varies from 0% (clean sand) to 60%. The small squares demonstrate P-wave velocity change with clay content for a sandstone with 32.06% original porosity and a pure shale with 20.38% porosity. Marion's (1992) porosity model was used here. The arrows show the direction of increasing clay content.



## Conclusions

1. Pore geometry (pore aspect ratio) can explain most of the scatter in the porosity–velocity relationship.
2. From this point of view, clays are associated with pores having much smaller aspect ratios than those associated with sands.
3. The effect of clays can be approximated using the clay–sand mixture model presented here.
4. The time-average model and the Raymer *et al.* (1980) equation for hard formations provide meaningful results only for clean formations containing pores with a mean aspect ratio of about 0.1.
5. Application of the new clay–sand mixture model shows that the mean aspect ratios are in the range 0.02–0.05 for clay-related pores, around 0.12 for sand-related pores and 0.1 for carbonate-related pores.

## Acknowledgements

The authors are indebted to the sponsors of the Birkbeck College Research Programme in Exploration Seismology: Amoco (UK) Exploration Company, BP Exploration Operating Company Ltd., Enterprise Oil plc, Fina Exploration Ltd., GECO Geophysical Company Ltd., Mobil North Sea Ltd., Sun Oil Britain Ltd. and Texaco Britain Ltd. for their support of this research. We thank the referees for their help in improving the paper. This is publication number 50 of the Birkbeck College & UCL Research School of Geological and Geophysical Sciences.

## Appendix A

### *Porosity evaluation from logging data*

In order to study the porosity–velocity behaviour using logging data, the porosity should first be evaluated from one of the porosity logs or a combination of them. Archie (1942) first related resistivity of a porous rock to porosity. However, the well-known Archie equation is valid only for clean (clay-free) formations. Bussian (1983) proposed a relationship for the resistivity of clay sands in terms of the electrical properties of any heterogeneous mixture of two components. Dos Santos, Ulrych and de Lima (1988) employed Bussian's (1983) resistivity model and the Wyllie *et al.* (1956) velocity model to relate the transit times of shaly formations to their electrical properties. Bussian's (1983) model was recently modified by Xu and White (1992, as above) to take full account of the effect of clays on the formation resistivity. In terms of the modified Bussian model, one can estimate the porosity of shaly formations as follows:

1. Shale volume is evaluated from gamma ray logs, or other shale indicators, by a standard technique.

2. An analogue of Archie's law is used to predict the effect of clay on  $R_r$ , the resistivity of the mixture of matrix grains with shales.
3. The modified Bussian's equation is used to evaluate porosity.

An advantage of using resistivity logs to evaluate porosity is that most of the common minerals except clays are electrically resistive and, apart from clays, porosity measurements from resistivity logs are largely insensitive to lithology variations. One uncertainty associated with porosity evaluation from resistivity logs comes from poor knowledge about  $R_w$ , the resistivity of the pore fluid. Density and neutron logs are the other porosity indicators. If either one (or both) of them is available, comparison of the porosities estimated from both resistivity and density (or neutron) logs can provide a sensible value of  $R_w$ .

## Appendix B

### *Scalars in the Kuster and Toksöz (1974) theory*

The scalars  $T_{üijj}$  and  $T_{ijij}$  which are used in text are given by

$$T_{üijj} = \frac{3F_1}{F_2},$$

$$T_{ijij} - \frac{1}{3}T_{üijj} = \frac{2}{F_3} + \frac{1}{F_4} + \frac{F_4F_5 + F_6F_7 - F_8F_9}{F_2F_4},$$

where

$$F_1 = 1 + A[\frac{3}{2}(g + \phi) - R(\frac{3}{2}g + \frac{5}{2}\phi - \frac{4}{3})],$$

$$F_2 = 1 + A\left[1 + \frac{3}{2}(g + \phi) - \frac{R}{2}(3g + 5\phi)\right] + B(3 - 4R) \\ + \frac{A}{2}(A + 3B)(3 - 4R)[g + \phi - R(g - \phi + 2\phi^2)],$$

$$F_3 = 1 + \frac{A}{2}\left[R(2 - \phi) + \frac{1 + \alpha^2}{\alpha^2}g(R - 1)\right],$$

$$F_4 = 1 + \frac{A}{4}[3\phi + g - R(g - \phi)],$$

$$F_5 = A[R(g + \phi - \frac{4}{3}) - g] + B\phi(3 - 4R),$$

$$F_6 = 1 + A[1 + g - R(g + \phi)] + B(1 - \phi)(3 - 4R),$$

$$F_7 = 2 + \frac{A}{4}[9\phi + 3g - R(5\phi + 3g)] + B\phi(3 - 4R),$$

$$F_8 = A\left[1 - 2R + \frac{g}{2}(R - 1) + \frac{\phi}{2}(5R - 3)\right] + B(1 - \phi)(3 - 4R),$$

$$F_9 = A[g(R - 1) - R\phi] + B\phi(3 - 4R),$$

$$A = \frac{\mu'}{\mu} - 1,$$

$$B = \frac{1}{3} \left( \frac{K'}{K} - \frac{\mu'}{\mu} \right),$$

$$R = \frac{3\mu}{3K + 4\mu},$$

$$g = \frac{\alpha^2}{1 - \alpha^2} (3\phi - 2),$$

$$\phi = \frac{\alpha}{(1 - \alpha^2)^{3/2}} [\cos^{-1} \alpha - \alpha(1 - \alpha^{1/2})]. \quad (\text{B1})$$

Here  $\alpha$  denotes aspect ratio;  $K$  and  $\mu$  denote the bulk and shear moduli of the solid in which the pores are embedded;  $K'$  and  $\mu'$  are the bulk and shear moduli of the inclusions.

## References

- Anstey N.A. 1991. Velocity in thin section. *First Break* 9, 449–457.
- Archie G.E. 1942. The electrical resistivity log as an aid in determining some reservoir characteristics. *Petroleum Technology* 1, 55–67.
- Bussian A.E. 1983. Electrical conductance in a porous medium. *Geophysics* 48, 1258–1268.
- Cheng C.H. and Toksöz M.N. 1979. Inversion of seismic velocities for the pore aspect ratio spectrum of a rock. *Journal of Geophysical Research* 84, 7533–7543.
- Dos Santos W.L.B., Ulrych T.J. and De Lima O.A.L. 1988. A new approach for deriving pseudovelocity logs from resistivity logs. *Geophysical Prospecting* 36, 83–91.
- Eastwood R.L. and Castagna J.P. 1983. Basis for interpretation of  $V_p/V_s$  ratios in complex lithologies. Proceedings of 24th SPWLA annual logging symposium, G1–G17.
- Eshelby J.D. 1957. The determination of the elastic field of an ellipsoidal inclusion, and related problems. *Proceedings of the Royal Society A* 241, 376–396.
- Gassmann F. 1951. Elasticity of porous media. *Vierteljahrsschrift der Naturforschenden Gesellschaft in Zürich* 96, 1–21.
- Han D., Nur A. and Morgan D. 1986. Effect of porosity and clay content on wave velocity in sandstones. *Geophysics* 51, 2093–2107.
- Hornby B.E., Schwartz L.M. and Hudson J.A. 1993. Effective medium modelling of the electrical and elastic properties of anisotropic porous media. 63rd SEG meeting, Washington, D.C., Expanded Abstracts, 786–791.
- Hudson J.A. 1981. Wave speed and attenuation of elastic waves in material containing cracks. *Geophysical Journal of the Royal Astronomical Society* 64, 133–150.
- Jordan J.R. and Campbell F.L. 1986. Well Logging II – Electric and Acoustic Logging. SPE, New York.
- Klimentos T. 1991. The effects of porosity-permeability-clay content on the velocity of compressional waves. *Geophysics* 56, 1930–1939.

- Klimentos T. and McCann C. 1990. Relationships between compressional wave attenuation, porosity, clay content, and permeability of sandstones. *Geophysics* 55, 998–1014.
- Krief M., Garat J., Stellingwerff J. and Ventre J. 1990. A petro-physical interpretation using the velocities of P- and S-waves (full-waveform sonic). *The Log Analyst* 31, 355–369.
- Kuster G.T. and Toksöz M.N. 1974. Velocity and attenuation of seismic waves in two phase media: Part 1: Theoretical formulation. *Geophysics* 39, 587–606.
- Marion D., Nur A., Yin H. and Han D. 1992. Compressional velocity and porosity in sand-clay mixtures. *Geophysics* 57, 554–563.
- Nishizawa O. 1982. Seismic velocity anisotropy in a medium containing oriented cracks – transversely isotropic case. *Journal of the Physical Earth* 30, 331–347.
- Nur A. 1971. Effects of stress on velocity anisotropy in rocks with cracks. *Journal of Geophysical Research* 76, 2022–2034.
- O'Connell R.J. and Budiansky B. 1974. Seismic velocities in dry and saturated cracked solid. *Journal of Geophysical Research* 79, 5412–5426.
- Raymer L. L., Hunt E.R. and Gardner J.S. 1980. An improved sonic transit time to porosity transform. Proceedings 21st SPLWA annual logging symposium, Paper P.
- Reuss A. 1929. Berechnung der fließgrenze von mischkristallen auf grund der plastizitätsbedingung für einkristalle. *Zeitschrift für Angewandte Mathematik und Mechanik* 9, 49–58.
- Rider M.H. 1986. *The Geological Interpretation of Well Logs*. Blackie and Son Limited, Glasgow.
- Tao G. and King M.S. 1993. Porosity and pore structure from acoustic well logging data. *Geophysical Prospecting* 41, 435–451.
- Tatham R.H. 1982.  $V_p/V_s$  and lithology. *Geophysics* 47, 336–344.
- Toksöz M.N., Cheng C.H. and Timur A. 1976. Velocities of seismic waves in porous rocks. *Geophysics* 41, 621–645.
- White J.E. 1965. *Seismic Waves: Radiation, Transmission, and Attenuation*. McGraw-Hill Book Co.
- Wood A.W. 1941. *A Textbook of Sound*. Macmillan Publishing Co.
- Wu T.T. 1966. The effect of inclusion shape on the elastic moduli of a two-phase material. *International Journal of Solids Structure* 2, 1–8.
- Wyllie M.R., Gregory A.R. and Gardner L.W. 1956. Elastic wave velocities in heterogeneous and porous media. *Geophysics* 21, 41–70.
- Zimmerman R.W. 1984. *The effect of pore structure on the pore and bulk compressibility of consolidated sandstones*. Ph.D. thesis, University of California, Berkeley.